INLET RECIRCULATION IN PARTLOAD REGIMES – RADIAL PUMP

PROKOP MORAVEC[1], LUKAS ZAVADIL[2], JAKUB STARECEK[1], TOMAS KRATKY[1], TOMAS DANEK[2], PETR ABRAHAMEK[2]

[1]CENTRE OF HYDRAULIC RESEARCH,

[2]SIGMA Research & Development Institute,

Lutin, Czech Republic

DOI: 10.17973/MMSJ.2022_06_2022060

p.moravec@sigma.cz

Partload regimes of all types of centrifugal pumps are strongly and unfavorably affected by an influence of an inlet recirculation. This negative phenomenon usually occurs at pump suctions, when a circumferential velocity component of the fluid flow (derived from a rotational speed of a rotor) is dominant over an axial velocity component. Such physical effect goes hand in hand with a creation of a pump-head instability, a decrease of an overall efficiency, an excessive noise and pressure pulsations and even a possible cavitation formation. The introduced technical problem was tested/examined for a radial centrifugal pump Ns375 with a volute (spiral casing) and an axial intake domain with two potential countermeasures. Both, a physical experiment and transient numerical simulations were employed and compared on crucial levels.

KEYWORDS

Radial pump, inlet recirculation, partload regime, unsteady flow, volute, CFD, pump-head instability, SST-SAS model.

1 INTRODUCTION

At certain values of the volume flow rate (usually at the partload regimes of the examined hydraulic machine), all the centrifugal pumps develop the internal flow recirculation in the suction and also in the discharge of the rotating impeller. The internal recirculation phenomenon generates intensive and complex 3D vortical structures with high fluid velocities, which cause a significant static pressure lowering at that specific location. This fact can lead to the creation of the cavitation, excessive noise/vibrations or pressure pulsations. It must be noted/considered that the major increase of an inlet diameter of the impeller during a design process results in a decrease of the entrance velocity (circumferential velocity starts to be the dominant factor in the main fluid flow) – the working medium tends to almost reverse itself and flow out of the pump suction [Karassik 1998].

Generally, there are two principal ways of reducing (at least shifting from the requested operational range) the inlet recirculation problem in the centrifugal pumps: first, by a proper design of the pump impeller (found e.g. in [Breugelmans 1982] [Lipej 2016]) and second, by built-in structures or modifications located in the front of the impeller (found in e.g. [Predin 2003], [Lin 2022]). The second option was tested in the proposed research by utilizing two counter-measuring methods/modifications – a simple cross structure and shallow radial grooves (in more detail in Chapter 2).

The presented research was built upon a knowledge from a grant project – Suppression of negative effects of inflow recirculation in high-capacity cooling pumps, where an open (without a rotating shroud disc) pump impeller with 5 blades and a volute were designed under a model name **Ns375** (name is derived from the result of Equation 1). A design point of the mentioned pump is summarized by the following table (Table 1).

	Value	Unit
Volume flow rate Q_{opt}	335	m^3/s
Pump head H	23.5	m
Shaft (rotational) speed n	1 900	RPM

Table 1. Pump design point

The pump design point data in Table 1 could be transformed for a proper pump comparison into a specific speed n_s (min^{-1}) [Paciga 1984]:

$$n_s = 3.65 \cdot n \cdot \frac{Q^{0.5}}{H^{0.75}} \approx 375\ min^{-1}, \quad (1)$$

or a specific speed n_q (min^{-1}) [Gulich 2014]:

$$n_q = n \cdot \frac{Q^{0.5}}{H^{0.75}} \approx 103\ min^{-1}. \quad (2)$$

2 PUMP GEOMETRY

A complete pump assembly of Ns375 with the volute, which was examined in this research, is shown in Figure 1. Inside parts (water/fluid domains) were modelled afterwards in SolidWorks environment for purposes of the numerical simulations.

The pump impeller was designed as open – without the rotating shroud. A tip gap between the rotor (blades) and the stator (casing) was set as a constant and equaled to 0.3 mm.

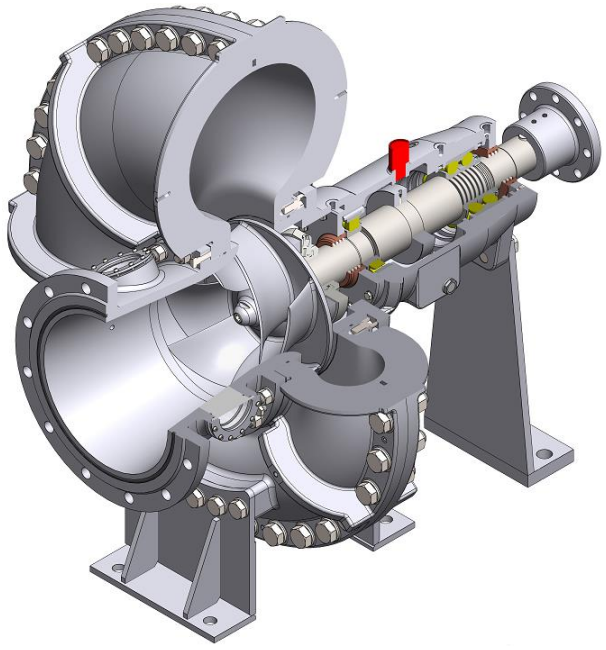

Figure 1. Complete pump assembly

2.1 Intake domain modifications

The main dimensions of the original intake domain (without the modifications) are shown in Figure 2.

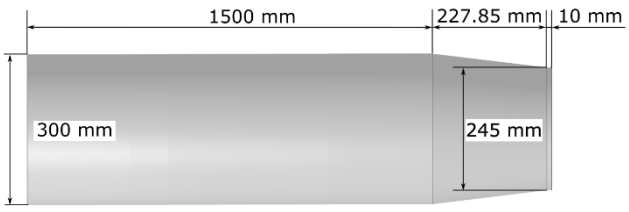

Figure 2. Main dimensions of the intake domain (without modifications)

Three different types of intake domains were thoroughly examined, namely: the intake domain without the modifications (Figure 2; represented in the following text/graphs/visualizations by a red color); the intake domain with several shallow radial grooves (Figure 3; green color) and the intake with the built-in cross structure (Figure 4; blue color). Both of the inlet recirculation countermeasures were located/restricted in a convergent part of the intake domain. It must be noted that only a type without the modifications was supported by the measurement (physical experiment) in a hydraulic laboratory.

The radial groove modification (Figure 3) could be summarized by following basic dimensions:

- Width of the individual groove: $s = 10\ mm$.
- Depth of the individual groove: $h = 5\ mm$.
- Number of grooves: $p = 11$.

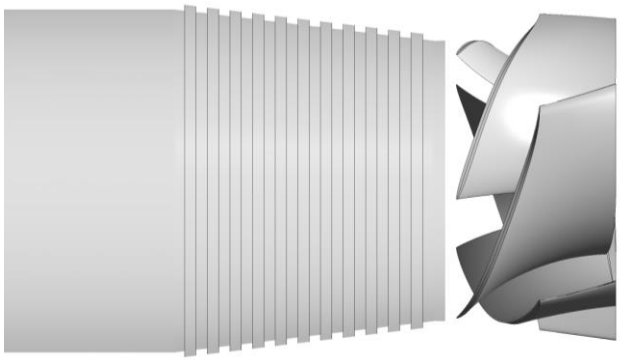

Figure 3. Radial grooves

The cross structure modification (Figure 4) could be summarized by following basic dimensions:

- Cross blade thickness: $\Delta = 10\ mm$.
- Axial length of the cross: $l = 207.85\ mm$.
- Axial position from the end of the intake domain (interface rotor-stator): $z_{out} = 20\ mm$.
- Leading/trailing edge radius: $R = 5\ mm$.

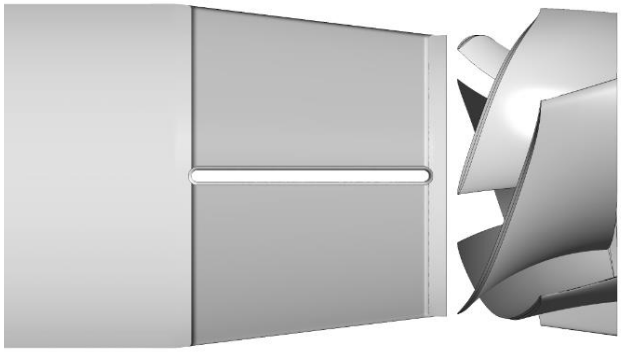

Figure 4. Cross structure

3 NUMERICAL SIMULATIONS

A commercial software package ANSYS 2019 R3 was extensively utilized in this research for the steady/transient numerical simulations of the fluid flow and for the necessary additional procedures connected with them (computational mesh generation, case pre/post-processing).

3.1 Computational mesh

The computational mesh of all work-flow subdomains (see the mesh sample in Figure 5), namely: the intake domain and the volute were created in ANSYS Workbench meshing as tetrahedral with high-resolution prismatic layers near the solid walls; the hexahedral mesh was utilized for the pump impeller in TurboGrid, and ANSYS Workbench meshing and its hexahedral elements was used for a partially enclosed space behind the pump hub.

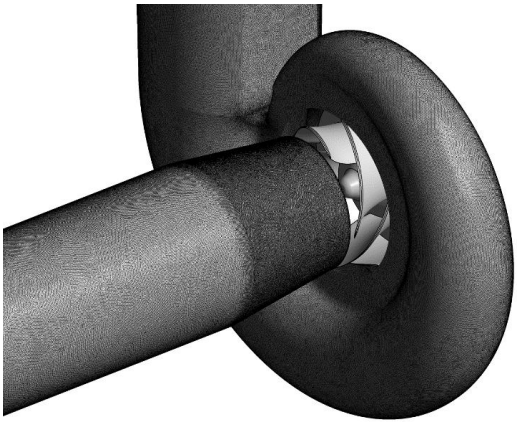

Figure 5. Sample of the computational mesh (SAS-SST)

Utilized computational mesh sizes are summarized by the following Table 2, where total numbers of nodes and elements are enumerated.

	Nodes	Elements
Axial intake (SAS-SST)	17 421 473	56 114 395
Radial grooves (SAS-SST)	17 435 020	56 679 903
Cross (SAS-SST)	18 324 848	59 828 940

Table 2. Computational mesh sizes

3.2 CFD solver setup

A complete computational model of the pump Ns375 is shown in a following scheme – Figure 6, where the 5-blade pump impeller was the only rotational domain (without the rotating shroud) with a transient rotor-stator type of the interface towards the intake and the volute. The axis of the rotation was aligned with the global z-axis in the computational model.

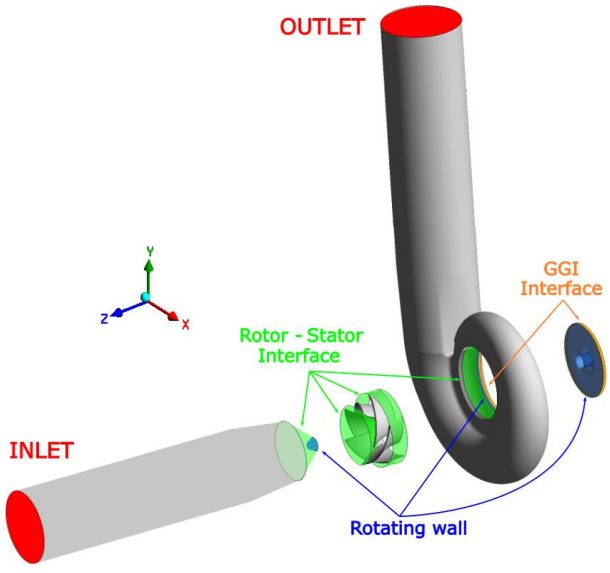

Figure 6. Computational model of the pump (working domains)

The partially enclosed space behind the pump hub was connected with the volute domain by using a GGI type of interface. Blue surfaces in Figure 6 were prescribed as rotating walls with the same direction and RPM as the impeller (a part of the hub in the intake and the volute; a part of the hub behind the impeller). The zero total pressure was set as the inlet boundary condition; the outlet boundary condition utilized a mass flow rate (kg/s), which corresponded with examined values of the volume flow rate (Q/Q_{opt}). The reference pressure was in all computational domains 1 atm (101 325 Pa). All solid walls were modelled as hydraulically smooth. The working medium was water at 25°C with a density 997 kg/m^3 and a dynamic viscosity 889.9 µPa·s (more detailed material properties could be found in [ANSYS 2019] – Water at 25°C). The fluid flow was one-phased, incompressible and isothermal.

A SST-SAS model of turbulence was exploited in the numerical simulations of the fluid flow inside the main domains of the pump with an automatic wall function. A timestep for the SST-SAS model of turbulence corresponded to 1° of the pump impeller revolution with 3-5 inner iterations.

3.3 Case evaluation

Two crucial performance characteristics were evaluated in all CFD simulations. First, a pump head H (m) [IEC 60 193]:

$$H = \frac{p_{total,outlet} - p_{total,inlet}}{\rho g}, \quad (3)$$

where $p_{total,outlet}$ (Pa) is a total pressure at the domain outlet (Figure 6); $p_{total,inlet}$ (Pa) is a total pressure at the domain inlet (Figure 6); ρ (kg/m^3) is the water density and g (m/s^2) is a gravitational acceleration. This quantity was morphed in ANSYS CFX PRE into a following form (CFX expression):

*(massFlowAve(Total Pressure in Stn Frame)@OUTLET - massFlowAve(Total Pressure in Stn Frame)@INLET) / (997 * g).*

A hydraulic efficiency η_H (%) [IEC 60 193]:

$$\eta_H = \frac{(p_{total,outlet} - p_{total,inlet}) \cdot Q}{2\pi n M_k} \cdot 100, \quad (4)$$

where $p_{total,outlet}$ (Pa) is the total pressure at the domain outlet (Figure 6); $p_{total,inlet}$ (Pa) is the total pressure at the domain inlet (Figure 6); Q (m^3/s) is the volume flow rate, n (1/s) is the shaft rotational speed and M_k (Nm) is a torque. This quantity was morphed in ANSYS CFX PRE into a following form (CFX expression):

*(((massFlowAve(Total Pressure in Stn Frame)@OUTLET - massFlowAve(Total Pressure in Stn Frame)@INLET) * Q) / (2 * pi * 1900 * torque)) * 100.*

A definition of the circumferential velocity v_{circ} (m/s) must be added to a proper case evaluation of the given problem:

$$v_{circ} = \sqrt{v_x^2 + v_y^2}, \quad (5)$$

where v_x (m/s) is the x-component of the velocity (see the global axis definition in Figure 6); v_y (m/s) is the y-component of the velocity. This quantity was morphed in ANSYS CFX PRE into a following form (CFX expression):

sqrt(Velocity in Stn Frame u^2 + Velocity in Stn Frame v^2).

It must be noted:

- A steady state RANS calculation of the fluid flow with a frozen rotor type of interface between the stationary and the rotational parts of the pump served for a basic transient simulation initialization.
- *massFlowAve* computes the average of a variable on the specified location (plane, surface) weighted by the mass flow at each point (node) on this location. For more detail see [ANSYS 2019].
- Individual values of the performance characteristics as well as selected variables were averaged from **9-16** revolutions of the pump impeller n_{ex} (-) (Figure 7).

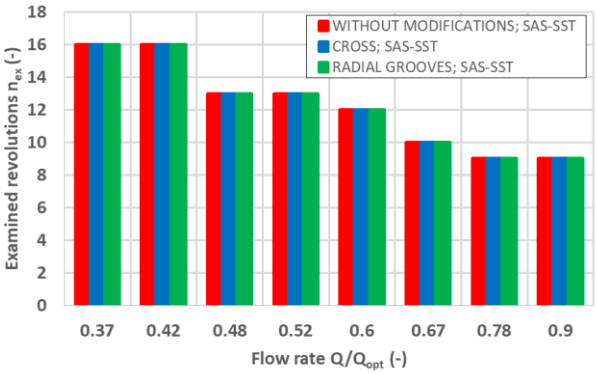

Figure 7. Numbers of evaluated revolutions (case by case comparison)

- The mentioned physical measurement was done **only** for the pump with the intake domain, which does not include any types of the modifications.

4 RESULTS

4.1 Comparison with experimental data

A data comparison with the physical experiment is shown in Figure 8 and 9 – the pump head and the efficiency dependencies on the dimensionless flow rate Q/Q_{opt} (-).

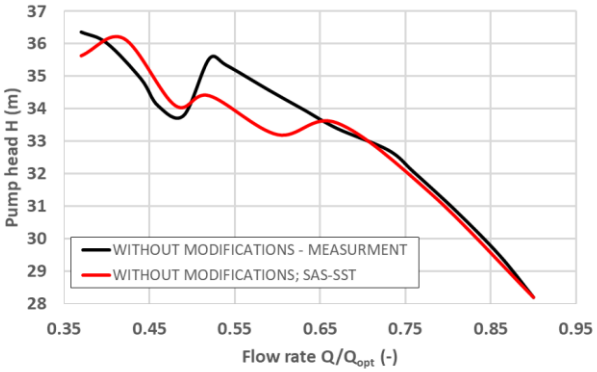

Figure 8. H – Q/Q_{opt} dependency

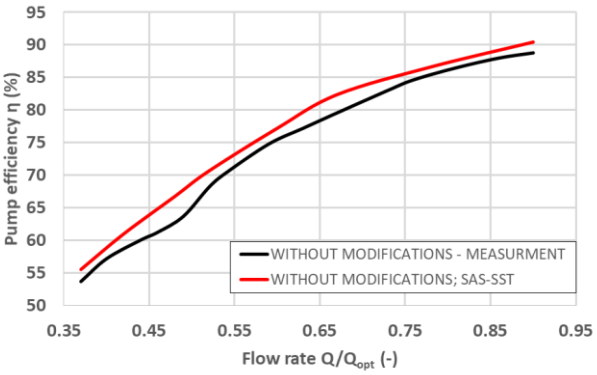

Figure 9. η – Q/Q_{opt} dependency (η_H for CFD)

The numerical simulations of the pump Ns375 tended to predict the pump-head instability at higher/bigger values of the flow

rate, to be more specific at the pump regime defined by the flow rate Q/Q_{opt} = 0.6, compared to Q/Q_{opt} = 0.48 from the experiment. This discrepancy in the pump head may have been mainly due to the simplified pressure evaluation in the CFD simulations, i.e., averaging the data (total pressure) from the chosen surfaces (see section 3.3) versus averaging the data (static pressure) from pressure sensors in a circular arrangement (experiment); and partially due to the potential influence of the cavitation caused by the dominant effect of the circumferential velocity. A curve trend around the main (sharp) pump head instability (located in Q/Q_{opt} = 0.48) was estimated sufficiently accurate.

The pump efficiency (the total efficiency of the pump from the experiment vs. the hydraulic efficiency from CFD) is for all examined values of the flow rate assessed well by CFD with a minor value overestimation mainly due to a neglecting of motor/bearing mechanical losses.

It must be also mentioned that all CFD simulations were **only** created as one-phased (water as the working medium) – the cavitation in the working domains was completely disregarded. In the section 4.2 is a cavitation problem supported by a relative static pressure evaluation/rendering, where the reference pressure was set as 1 atm (101 325 Pa).

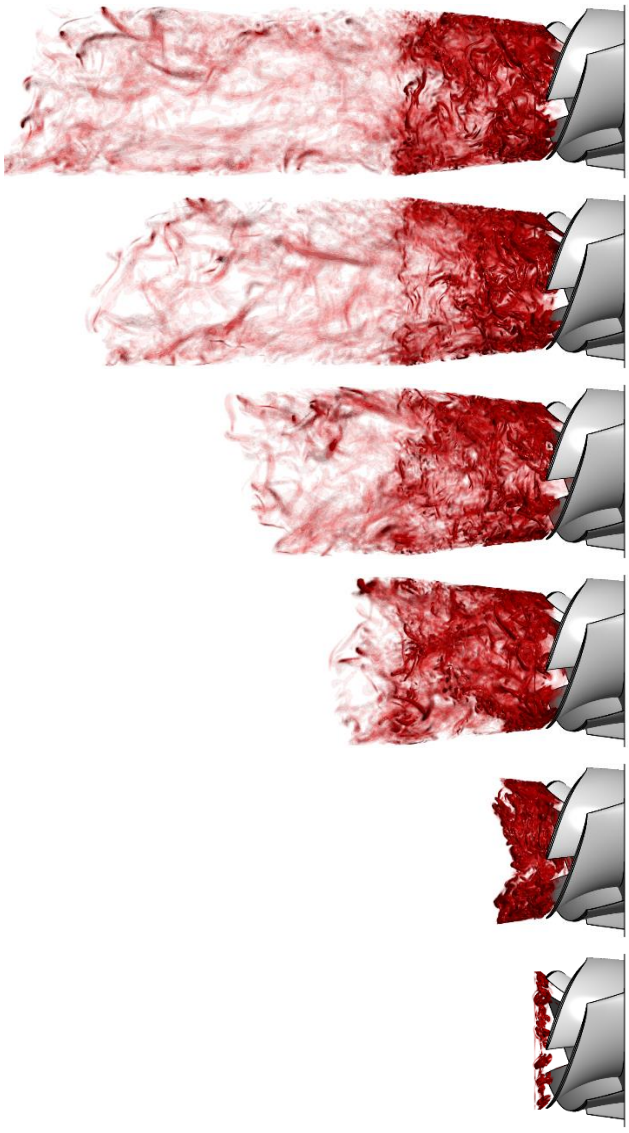

Figure 10. 3D vortical structures (final timestep); Q/Q_{opt} = 0.37 – 0.67

A six-piece set of pictures in Figure 10 demonstratively illustrates a gradual change of the axial position (the axial length) of the complex vortical structures in the intake domain of the examined pump (utilization of a swirl strength variable rendering from the final timestep of the transient simulations with same settings; for more detail about the swirl strength variable see [ANSYS 2019]). This axial position of the vortical structures is radically reduced by a flow rate Q/Q_{opt} increase, where the axial velocity component of the fluid flow started to prevail.

4.2 CFD data comparison (modification comparison)

Following graphs and figures/visualizations were created to compare the modifications against the inlet recirculation on several main levels, namely – the performance/force characteristics (Figure 11 – 13), a 3D complex vortical structure comparison in the selected values of the flow rate (Figure 14), an axial velocity rendering (for a backflow disclosure, Figure 21 – 26), a circumferential velocity (Figure 15 – 20) or a low relative static pressure manifestation to uncover potential spots and areas, where the cavitation could emerge (Figure 27 – 32).

Performance/force characteristics

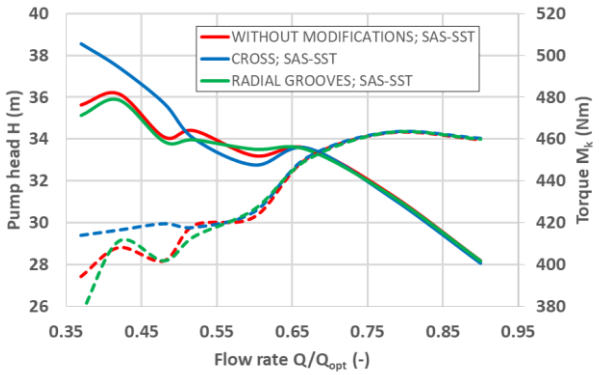

Figure 11. H – Q/Q_{opt} dependency (dashed line: M_k – Q/Q_{opt})

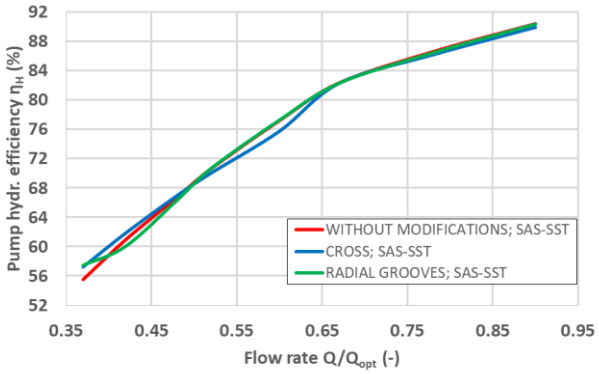

Figure 12. η_H – Q/Q_{opt} dependency

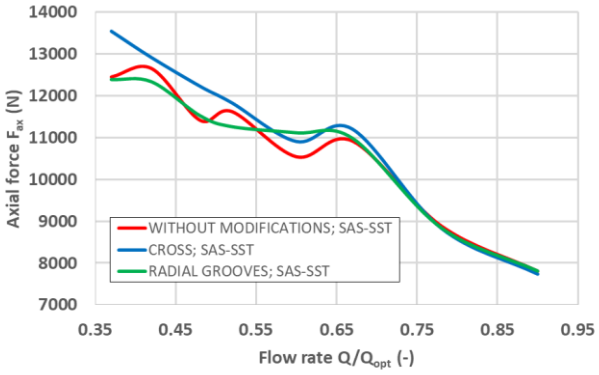

Figure 13. F_a – Q/Q_{opt} dependency

The numerical simulations of the fluid flow of all examined cases/types of the intake modifications predicted the pump-head instability (a pump-head curve drop) at the same flow rate interval 0.55 – 0.65 Q/Q_{opt} (Figure 11 – solid lines). This pump-head curve drop tended to be premature, when comparing it with the physical experiment with the intake with no modifications (see the flow rate – head dependencies in Figure 8). The modification with the shallow radial grooves tended to smooth out pump-head fluctuations in the flow rate interval 0.37 – 0.65 Q/Q_{opt} (Figure 11 – solid lines, when comparing with the intake without the modifications). The cross modification had the most visible/prominent pump-head curve drop and subsequently the most noticeable pump-head curve trend recovery. This so-called recovery is a result (partially) of a substantial suppression of the vortical structures (Figure 14).

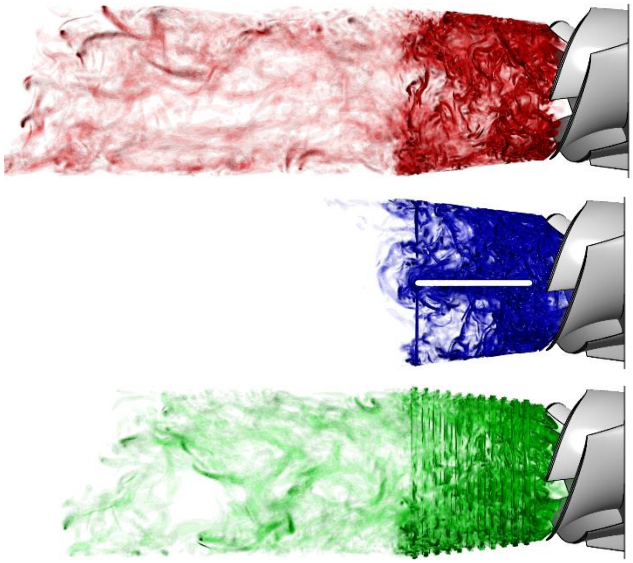

Figure 14. 3D vortical structures (final timestep); Q/Q_{opt} = 0.37

The shallow radial grooves and the simple cross structure placed in the pump intake did not have a significant impact on the hydraulic efficiency (Figure 12) in all examined values of the flow rate. In particular, the small impact in 0.37 – 0.48 Q/Q_{opt} is explained by the increased/decreased torque (Figure 11 – the comparison of the pump head and the torque). For the case of the cross, inlet conditions were improved (see Figure 14 and sections below) and therefore the pump head and the torque have increased (the other way around for the shallow grooves) – hence, Equation 4 produced similar values of the hydraulic efficiency for both cases. The small impact in the rest of the examined flow rate values was caused mainly due to the undeformed velocity triangle at the pump impeller inlet and a similar local (minor) loss of the modifications.

The CFD estimation of the axial force in the flow rate interval 0.37 – 0.65 Q/Q_{opt} (Figure 13) exposed a force value fluctuation in the case of no modifications intake. The pump-head instability of all types of the intake modification is partially propagated as well into a shape of the axial force dependency. It must be mentioned that positive values of the axial force denoted a proper force direction, which is aligned with the positive z-axis of the computational model (see the axis definition in Figure 6).

As it was briefly mentioned in the introduction of this article, the inlet recirculation goes hand in hand with the dominant influence of the circumferential velocity and a sectional reversal of the fluid flow. These two accompanying physical phenomena of the inlet recirculation were properly visualized and afterwards confirmed by following sets of pictures (Figure 15 – 32).

Circumferential velocity

The Figures 15 – 20 are focused on the circumferential velocity of the fluid flow in the intake domain of the examined centrifugal pump (see Equation 5) – contours of the examined variable were plotted from the final timestep (a top picture) and as a time-average (a bottom picture; for more detail about the variable averaging see Figure 7 and the text in a close surrounding of the figure). The mentioned contours were clipped in a closed working velocity range from 0 to 20 m/s for all types of the modifications. Axial length indicators were plotted in the bottom pictures (0 m, 0.4 m, 0.8 m), where the 0 m mark was placed in the beginning of the interface between the intake domain and the rotating domain of the pump impeller.

A rotated YZ plane, constructed only in the intake domain, was utilized for the variable visualization. It was rotated by 45° around the z-axis to avoid a major collision with the cross structure. Water flows from the left to the right, the contours of the circumferential velocity show only a magnitude not a possible direction.

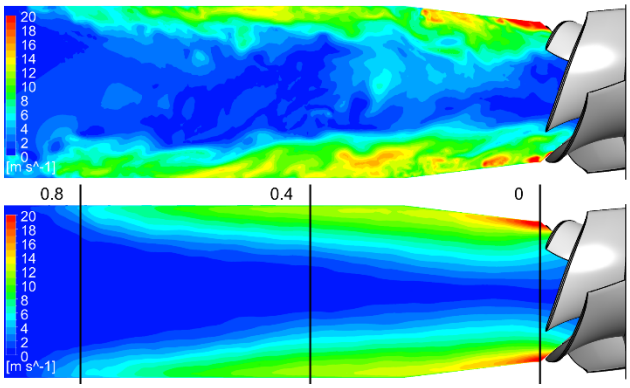

Figure 15. Circumferential velocity – no modifications; Q/Q_{opt} = 0.37

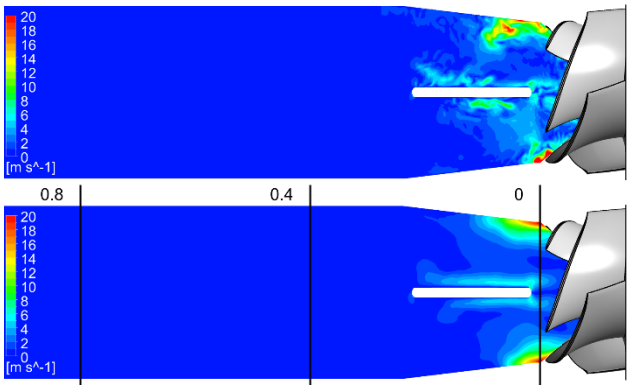

Figure 16. Circumferential velocity – cross structure; Q/Q_{opt} = 0.37

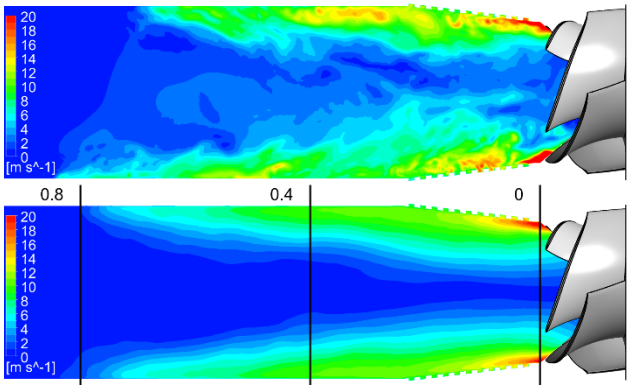

Figure 17. Circumferential velocity – radial grooves; Q/Q_{opt} = 0.37

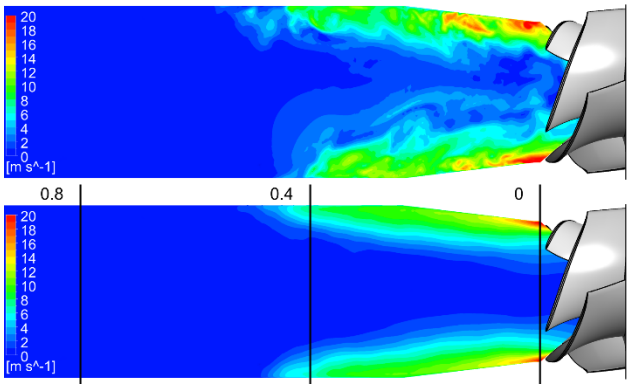

Figure 18. Circumferential velocity – no modifications; Q/Q_{opt} = 0.48

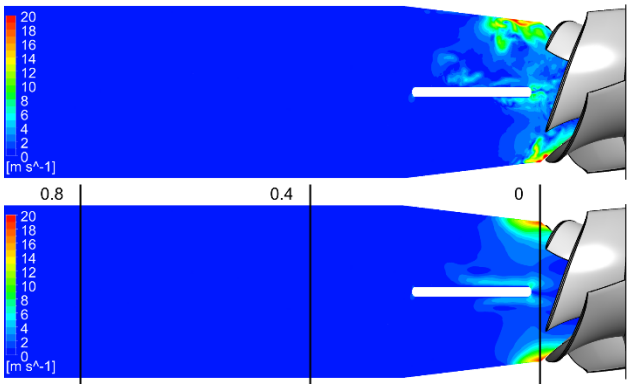

Figure 19. Circumferential velocity – cross structure; Q/Q_{opt} = 0.48

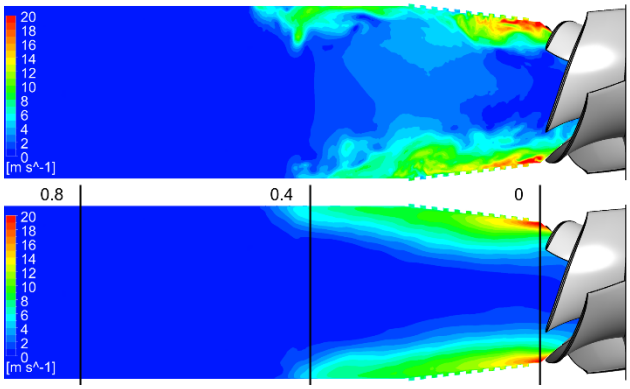

Figure 20. Circumferential velocity – radial grooves; Q/Q_{opt} = 0.48

It is distinctively noticeable that the circumferential velocity contours for the smallest value of the examined flow rate Q/Q_{opt} = 0.37 (Figure 15 – 17) revealed extremely unsteady and dissipative flow patterns in the model cases with no modifications and with the shallow radial grooves compared with the case with the cross structure, where the major eddy suppression took place.

The variable averaging process created a cone shape of the high values of the circumferential velocity with a core where, on the other hand, the axial velocity with a direction towards to the rotating impeller dominated. This effect resulted in a deformation of the velocity triangle at the pump impeller inlet (especially on an outer streamline), leading to an unsuitable fluid entry at the leading edge of the blade and a consequent alternation of the performance characteristics (hydraulic efficiency, pump head).

A comparison of the average values of the case with no modifications and with the shallow radial grooves showed following: the axial length of the cone shape is approximately the same; warm colors, which represented the high variable values, tended to be smaller in the case with the radial grooves.

Axial velocity (reversal flow)

The following Figures 21 – 26 are focused only on the axial velocity of the fluid flow in the intake domain of the examined centrifugal pump – the contours of examined variable were plotted from the final timestep (a top picture) and as a time-average (a bottom picture; for more detail about the variable averaging see Figure 7). The mentioned contours were clipped in a closed working velocity range from 0 to 5 m/s for all types of the modifications. The axial length indicators were plotted in the bottom pictures (0 m, 0.4 m, 0.8 m). It must be mentioned that only positive values of the axial velocity were plotted in Figure 21 – 26 due to the positive z-axis direction of the utilized computational model (the negative values were neglected; see the global axis definition in Figure 6) – thus water, which had the reversal movement against the main flow must have the positive values of the examined axial velocity.

The same variable evaluation YZ plane was used as in the previous subsection of the article (Circumferential velocity).

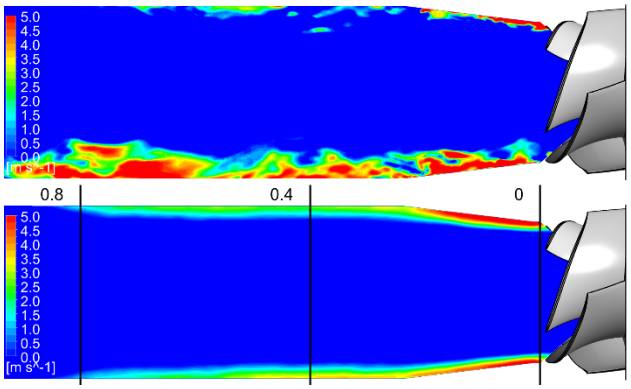

Figure 21. Axial velocity – no modifications; Q/Q_{opt} = 0.37

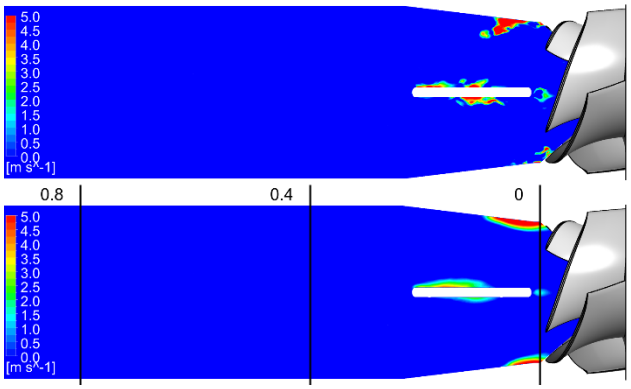

Figure 22. Axial velocity – cross structure; Q/Q_{opt} = 0.37

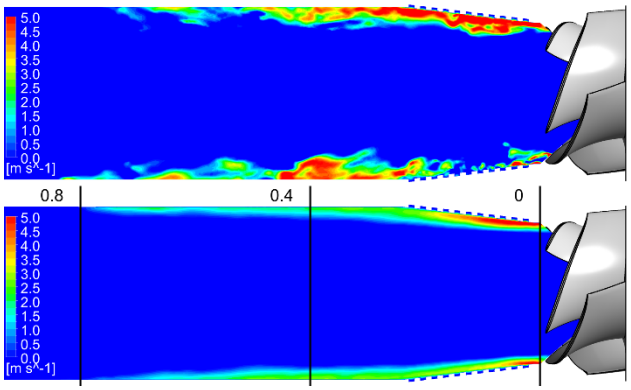

Figure 23. Axial velocity – radial grooves; Q/Q_{opt} = 0.37

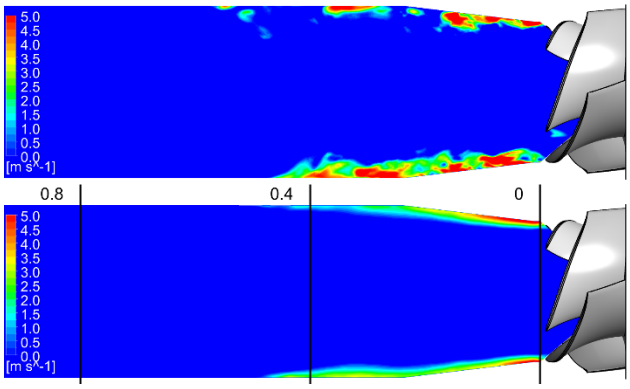

Figure 24. Axial velocity – no modifications; Q/Q_{opt} = 0.48

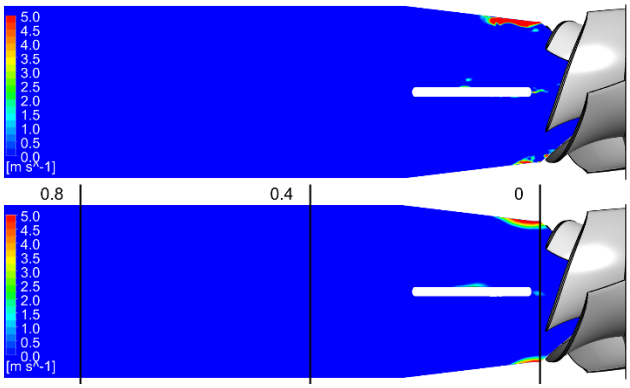

Figure 25. Axial velocity – cross structure; Q/Q_{opt} = 0.48

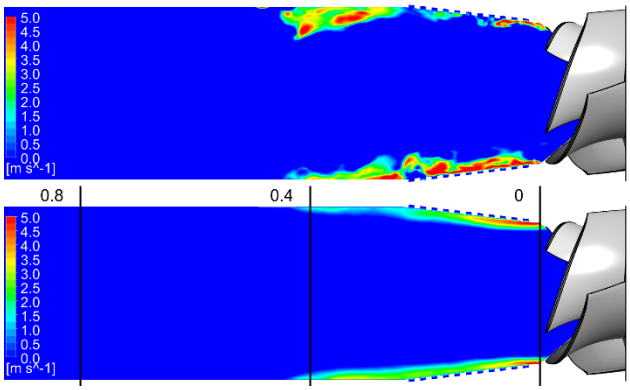

Figure 26. Axial velocity – radial grooves; Q/Q_{opt} = 0.48

The variable averaging process localized the backflow in a vicinity of the solid walls of the intake domain. As in the previous evaluation (subsection Circumferential velocity), the cross had the greatest effect on the backflow suppression at the pump impeller inlet. It should be noted that the shallow radial grooves tended to reduce the area of the maximal values of the positive axial velocity when compared to the unmodified model of the intake (see time-average comparisons).

Relative static pressure

The following Figures 27 – 32 are focused on the relative static pressure of the fluid flow in the intake domain of the examined centrifugal pump – the contours of the examined variable were plotted from the final timestep (a top picture) and as a time-average (a bottom picture; for more detail about the variable averaging see Figure 7). The mentioned contours were clipped in a closed working pressure range from -100 000 to 50 000 Pa for all types of the modifications. The axial length indicators were plotted in the bottom pictures (0 m, 0.4 m, 0.8 m).

The same variable evaluation YZ plane was used as in the previous subsections of the article.

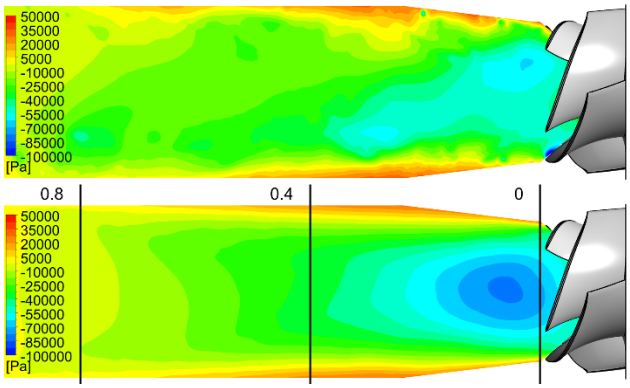

Figure 27. Static pressure – no modifications; Q/Q_{opt} = 0.37

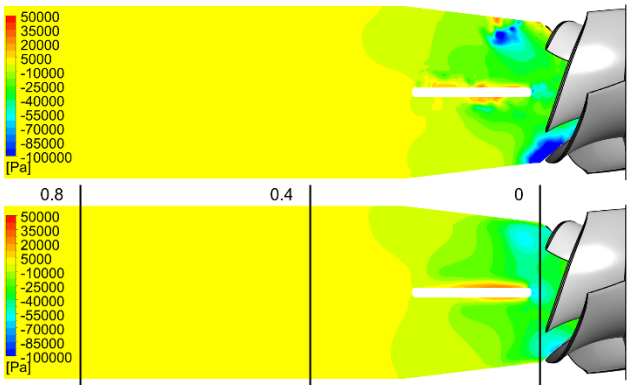

Figure 28. Static pressure – cross structure; Q/Q_{opt} = 0.37

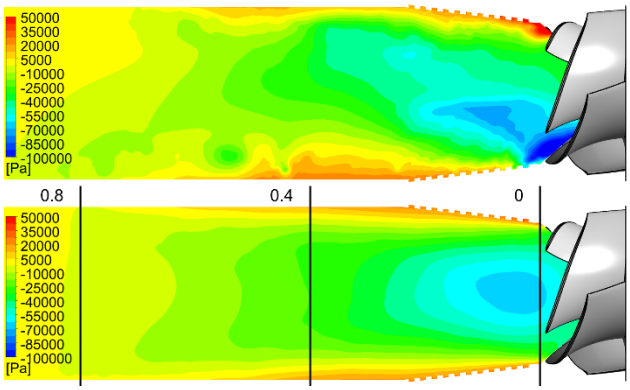

Figure 29. Static pressure – radial grooves; Q/Q_{opt} = 0.37

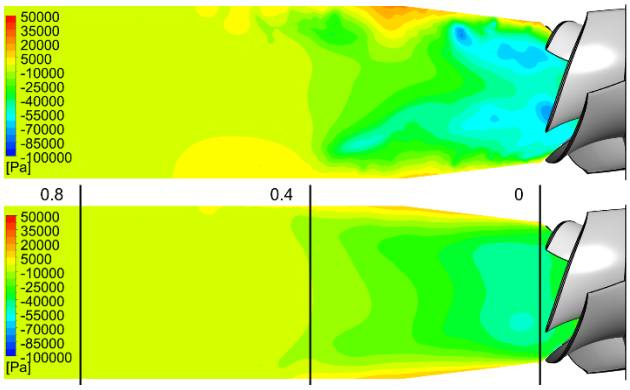

Figure 30. Static pressure – no modifications; Q/Q_{opt} = 0.48

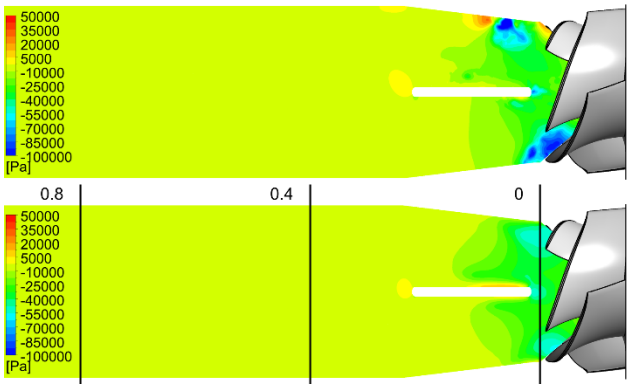

Figure 31. Static pressure – cross structure; Q/Q_{opt} = 0.48

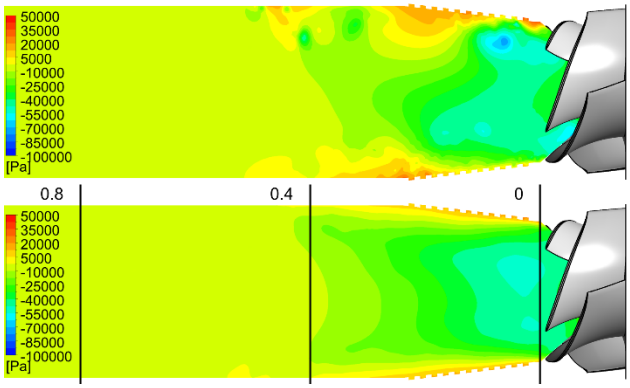

Figure 32. Static pressure – radial grooves; Q/Q_{opt} = 0.48

It must be mentioned that in the rendered contours existed spots/places, where the value of the static pressure dropped to (or below) -101 325 Pa. This phenomenon could indicate areas, where the cavitation can occur with a high probability. These places appeared to be in the open space of the intake and as well dangerously near the leading edge of the pump impeller.

5 CONCLUSIONS

This scientific paper summarizes the findings of the numerical flow simulations and the physical experiment on the inlet recirculation of the high-specific speed radial pump Ns375 with the circular cross-section volute. Two variants of the countermeasures against the manifestation of the recirculation embedded in the inlet domain of the named pump were extensively investigated: the less invasive shallow radial groove type, and the massive cross structure with ten millimeter thick blades. Both modifications were compared with the simple intake model based on the performance parameters (characteristics), the 3D vortex structures, the circumferential/axial velocities and the static relative pressure. The conclusions could be summarized:

- The numerical simulations (with the chosen SAS-SST model of turbulence and the additional settings) tended to prematurely predict the pump-head instability at the partload regimes of the pump; the shape and the trend of the efficiency curve was predicted accurately (when neglecting the mechanical losses in the bearings or in the motor).
- Both countermeasures did not have the significant impact on the examined hydraulic efficiency of the radial pump.
- The cross structure proved to be the most suitable in the suppressing the negative phenomena accompanying the inlet recirculation (the circumferential velocity, the vortex structures and the backflow) due to its invasive shape and size.
- The shallow radial groove modification showed promising results as the less invasive exploited countermeasure: it smoothed out the fluctuations in the pump head and in the axial force dependencies, and tended to mitigate the magnitude of the backflow when compared with the intake domain with no modifications.
- In all examined types of the intake model, the vortex structures formed with the significant decrease of the static pressure in their core – the creation of cavitation must be taken into account. For better problem understanding, it is necessary to utilize the two-phase computational model in the partload regimes of the pump.

ACKNOWLEDGMENTS

This research was supported by Ministry of Education, Youth and Sports of the Czech Republic under the project CZ.02.1.01/0.0/0.0/17 049/0008408 "Hydrodynamic design of pumps".

Computational resources were supplied by the project "e-Infrastruktura CZ" (e-INFRA CZ LM2018140) supported by the Ministry of Education, Youth and Sports of the Czech Republic and by the ELIXIR-CZ project (LM2018131), part of the international ELIXIR infrastructure.

REFERENCES

[Ansys 2019] ANSYS, Inc. ANSYS CFX User's Guide, Release 2019 R3.

[Breugelmans 1982] Breugelmans, F. A. E.; Sen, M. Prerotation And Fluid Recirculation In The Suction Pipe Of Centrifugal Pumps. Texas A&M University. Turbomachinery Laboratories, 1982. DOI: 10.21423/R1DM3B.

[Gulich 2014] Gulich, J.F. Centrifugal pumps. Heidelberg: Springer, 2014. ISBN 978-3-642-40113-8.

[IEC 60 193] International Standard IEC 60 193: Hydraulic pumps, and pump-turbines – Model acceptance tests. International Electrical Commission. Genf. 1999.

[Karassik 1998] Karassik, J., McGuire T. Centrifugal pumps. Springer, Boston, 1998. ISBN 978-1-4615-6606-9.

[Lin 2022] Lin, P., Yang, T., Xu, W., Zhu, Z. Influence of Different Offset Angles of Inlet Guide Vanes on Flow Characteristics of Centrifugal Pump. Frontiers in Energy Research. 2022. DOI: 10.3389/fenrg.2022.818244.

[Lipej 2016] Lipej, A., Mitrusevski, D. Numerical Prediction of Inlet Recirculation in Pumps. International Journal of Fluid Machinery and Systems, 2016, Volume 9, Issue 3. ISSN 1882-9554, DOI: 10.5293/IJFMS.2016.9.3.277.

[Paciga 1984] Paciga, A., Strycek O., Ganco M. Cerpacia technika. In Slovak. Bratislava: Alfa, 1984.

[Predin 2003] Predin, A., Bilus I. Influence of additional inlet flow on the prerotation and performance of centrifugal impellers. Journal of Hydraulic Research. 2003. DOI: 10.1080/00221680309499962.

CONTACT:

Ing. Prokop Moravec, Ph.D.
Department of Hydraulic Research
CENTRE OF HYDRAULIC RESEARCH, Jana Sigmunda 313, 783 49 Lutín
p.moravec@sigma.cz